Cell Reports



# Reduced Notch signaling in hypothalamic endothelial cells mediates obesity-induced alterations in glucose uptake and insulin signaling

## Graphical abstract

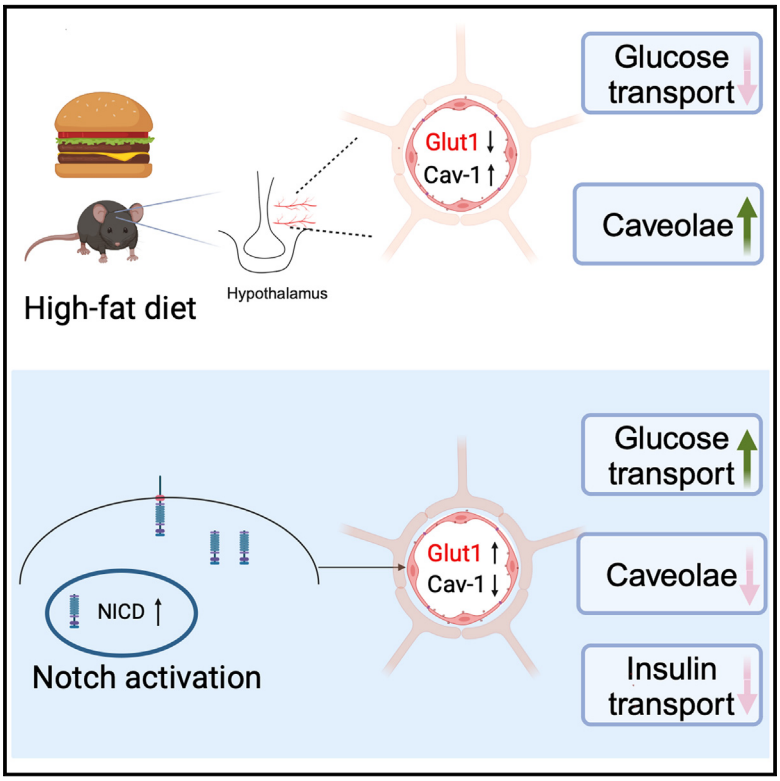


## Highlights

- HFD feeding reduces Notch1 expression in endothelial cells of the hypothalamus
- Endothelial Notch activation prevents HFD-induced reduction in glucose transport
- Endothelial Notch1 signaling regulates hypothalamic vascular permeability in obesity

## Authors

Yiyi Zhu, Oliver Mehlkop, Heiko Backes, ..., F. Thomas Wunderlich, Alexander Jais, Jens C. Brüning

## Correspondence

alexander.jais@helmholtz-munich.de (A.J.), bruening@sf.mpg.de (J.C.B.)

## In brief

Zhu et al. describe a rapid downregulation of Notch1 expression in hypothalamic blood-brain barrier (BBB) endothelial cells after high-fat diet (HFD) feeding. Notch activation prevents HFD-induced reduction of hypothalamic glucose uptake, highlighting a critical role of Notch signaling in the effects of short-term dietary transitions on BBB functionality.

Zhu et al., 2025, Cell Reports *44*, 115522
April 22, 2025 
https://doi.org/10.1016/j.celrep.2025.115522

CellPress

Cell Reports

CellPress
OPEN ACCESS

Report

# Reduced Notch signaling in hypothalamic endothelial cells mediates obesity-induced alterations in glucose uptake and insulin signaling

Yiyi Zhu,[1,2,3] Oliver Mehlkop,[1,2,3] Heiko Backes,[1] Anna Lena Cremer,[1] Marta Porniece,[1,2,3] Paul Klemm,[1,2,3] Lukas Steuernagel,[1,2,3] Weiyi Chen,[1,2,3] Ronja Johnen,[4] F. Thomas Wunderlich,[1] Alexander Jais,[1,2,3,5,*] and Jens C. Brüning[1,2,3,6,7,*]

[1]Department of Neuronal Control of Metabolism, Max Planck Institute for Metabolism Research, Gleueler Strasse 50, 50931 Cologne, Germany

[2]Cologne Excellence Cluster on Cellular Stress Responses in Aging-Associated Diseases (CECAD) and Center for Molecular Medicine Cologne (CMMC), University of Cologne, Köln, Germany

[3]Policlinic for Endocrinology, Diabetes and Preventive Medicine (PEDP), University Hospital Cologne, Kerpener Strasse 26, 50924 Cologne, Germany

[4]Cologne Excellence Cluster on Cellular Stress Responses in Aging-Associated Diseases (CECAD), Medical Faculty & Faculty of Mathematics and Natural Sciences, University of Cologne, Cologne, Germany

[5]Helmholtz Institute for Metabolic, Obesity and Vascular Research (HI-MAG) of the Helmholtz Zentrum München at the University of Leipzig and University Hospital Leipzig, Leipzig, Germany

[6]National Center for Diabetes Research (DZD), Ingolstädter Landstrasse 1, 85764 Neuherberg, Germany

[7]Lead contact

*Correspondence: alexander.jais@helmholtz-munich.de (A.J.), bruening@sf.mpg.de (J.C.B.)

https://doi.org/10.1016/j.celrep.2025.115522

## SUMMARY

Short-term transition to high-fat diet (HFD) feeding causes rapid changes in the molecular architecture of the blood-brain barrier (BBB), BBB permeability, and brain glucose uptake. However, the precise mechanisms responsible for these changes remain elusive. Here, we detect a rapid downregulation of Notch signaling after short-term HFD feeding. Conversely, Notch activation restores HFD-fed mouse serum-induced reduction of Glut1 expression and glycolysis in cultured brain microvascular endothelial cells (BMECs). Selective, inducible expression of the Notch intracellular domain (IC) in BMECs prevents HFD-induced reduction of Glut1 expression and hypothalamic glucose uptake. Caveolin (Cav)-1 expression in BMECs is increased upon short-term HFD feeding. However, NotchIC$^{BMECs}$ mice display reduced caveola formation and BBB permeability. This ultimately translates into reduced hypothalamic insulin transport, action, and systemic insulin sensitivity. Collectively, we highlight a critical role of Notch signaling in the pleiotropic effects of short-term dietary transitions on BBB functionality.

## INTRODUCTION

Local brain glucose transport is perturbed upon short-term high-fat diet (HFD) feeding, as evidenced by a significant reduction of Glut1 expression in brain microvascular endothelial cells (BMECs) and hypothalamic glucose uptake.[1,2] However, these studies have left open the important question of how HFD-induced obesity leads to Glut1 downregulation in BMECs.

In addition to glucose, energy-state-communicating hormones are transported into the brain via coordinated transport mechanisms. It has been shown that both insulin and leptin undergo saturable transport into the CNS.[3,4] While some studies have implicated insulin receptor expression in endothelial cells as a possible route for receptor-mediated transcytosis of insulin transport,[5] more recent studies have revealed that hypothalamic insulin uptake occurs largely independently of insulin receptor expression in BMECs.[6,7] In contrast, insulin receptor expression in tanycytes is required for insulin transport and its action in the arcuate nucleus of the hypothalamus (ARC).[6] Similarly, knockout of the insulin receptor gene in astrocytes disrupts insulin-dependent regulation of feeding,[8] further highlighting the role of insulin receptor expression in glial cells in the control of brain insulin action. However, it remains unresolved how insulin can pass endothelial cells to reach tanycytes and astrocytes. Noteworthy, caveolae have been closely linked to transcytosis as a potential mode of insulin transport. Here, inhibition of caveola formation can dose-dependently decrease insulin transport in endothelial cells.[9]

In the present study, we have performed *in situ* RNA gene expression analyses and a bacTRAP-based ribosomal profiling sequencing experiment to reveal that the downregulation of Notch signaling controls diet-induced changes of *Glut1* expression in BMECs. Inducible BMEC-selective Notch1 activation in mice (NotchIC$^{BMECs}$) prevents HFD-induced Glut1 suppression

as well as reduced hypothalamic glucose transport upon HFD feeding *in vivo*. In addition, Notch signaling in BMECs regulates Cav1 expression and caveola formation to acutely increase central insulin uptake in the hypothalamus and systemic insulin sensitivity during the early nutritional transition. Collectively, altered Notch signaling during nutritional transitions governs the pleiotropic mechanism in blood-brain barrier (BBB) permeability, brain glucose metabolism, and systemic insulin sensitivity.

## RESULTS

### Notch1 is downregulated in BMECs upon short-term HFD feeding

Short-term exposure to HFD decreases Notch1 expression in aortic endothelial cells.[10] Based on this, we first aimed at comparing Notch1 expression of BMECs of animals exposed to control diet (CD) or HFD feeding for 3 days. To achieve that, we quantified Notch1 expression in hypothalamic BMECs by *in situ* RNA hybridization. Interestingly, we found that 3 days of HFD is sufficient to induce a significant reduction of Notch1 expression in BMECs in the paraventricular nucleus of hypothalamus (PVH) (Figures 1A and 1B). Similarly, we observed significantly reduced Notch1 expression in BMECs in the ARC (Figures S1A and S1B).

Moreover, we employed a genetically modified mouse model, Slco1c1-CreERT2,[11] which expresses a tamoxifen-inducible variant of the Cre recombinase under the control of the Slco1c1 promoter to specifically mark BMECs (Figure S2A). These mice were crossed with ROSA26lSlL10aGFP mice to allow selective tamoxifen-inducible expression of a fusion protein of the ribosomal protein L10a with GFP (Figure S2A). As depicted in Figures S2A and S2B, Slco1c1CreERT2$^{tg/wt}$::ROSA26lSlL10aGFP$^{tg/wt}$ mice were treated with tamoxifen at the age of 12 weeks, allowing for the expression of L10aGFP selectively in BMECs. At the age of 15 weeks, the animals were subjected to either CD or HFD for 3 days. Thereafter, we collected hypothalami, performed anti-GFP immunopurification of L10aGFP-tagged ribosomes, and compared ribosome-associated mRNA expression in the immunoprecipitates (IPs). KEGG pathway analysis of differentially regulated genes between 3 days of CD and 3 days of HFD feeding revealed a downregulation of Notch signaling pathway components as well as *Glut1* expression in BMECs (Figures S2C and 4A). Together, the complementary approaches of *in situ* RNA analysis and ribosomal profiling recapitulated the diet-induced downregulation of *Glut1* expression and indicated reduced Notch signaling in BMECs upon short-term HFD feeding.

Next, we aimed to investigate whether the observed downregulation in Notch signaling could potentially represent a compensatory response to downregulated glucose transport and glycolysis in BMECs of HFD-fed mice. To this end, we incubated immortalized cerebral endothelial (cEND) cells with either vehicle or the Glut1 inhibitor WZB117[12] and subjected these cells to mRNA sequencing. Glut1 inhibition did not result in any alteration in the expression of Notch signaling components (Figures S3A and S3B). These data indicate that downregulated Notch signaling does not occur secondarily to reduced glucose uptake.

### Notch signaling regulates Glut1 expression and glucose metabolism in BMECs *in vitro*

We utilized cEND cells to investigate the effect of Notch signaling on Glut1 regulation. Application of the Notch activator Dll4 clearly promoted glycolysis in these cells (Figures S4A and S4B). Next, we found that incubating cEND cells for 24 h with serum from mice fed an HFD for 3 days resulted in a decrease in Glut1 protein expression compared to cells cultured in serum from CD-fed animals (Figures 2A and 2B). Interestingly, co-incubating cells cultured in serum from HFD-fed mice with Dll4 restored Glut1 expression (Figures 2A and 2B). Similarly, we observed a reduction in glycolytic capacity and glycolytic reserve in cEND cells incubated with serum from HFD-fed mice (Figures 2C and 2D). Moreover, simultaneous Notch activation restored the level of glycolytic rate of cEND cells in comparison to cells incubated with the serum of CD-fed mice (Figures 2C and 2D). Collectively, these data indicate that Dll4-mediated Notch activation can overcome the suppressive effect of serum from HFD-fed mice on Glut1 expression and glycolysis *in vitro*.

To identify the underlying mediator that could be responsible for diet-induced Notch1 and Glut1 downregulation, we measured serum concentrations of cholesterol and oxidized lipids in mice exposed to CD or HFD for 3 days. Of note, circulating total and free cholesterol concentrations were significantly elevated in mice exposed to HFD (Figure 2E). Moreover, we detected an increase in serum malondialdehyde (MDA) concentration as a measure of lipid oxidation (Figure 2E). Oxidized low-density lipoprotein (oxLDL) particles have previously been shown to reduce Notch signaling in human umbilical vein endothelial cells (HUVECs) and human aortic endothelial cells (HAECs).[10,13] Here, we found that oxLDL incubation reduced Glut1 protein expression in cultured BMECs, and this effect was reversed by Notch activation (Figures 2F and 2G). These data indicate that the increase of oxidized lipoprotein in animals fed a short-term HFD may contribute to the inhibition of Notch signaling and the subsequent reduction of Glut1 expression in BMECs.

### Notch signaling regulates Glut1 expression and glucose metabolism in BMECs *in vivo*

To define the contribution of Notch signaling to the metabolic reprogramming of BMECs *in vivo*, we subjected mice with constitutive Notch overactivation selectively in BMECs to a short-term nutritional challenge. To achieve this, we crossed Slco1c1-CreERT2 mice with those allowing for Cre-dependent expression of the Notch1 intracellular domain (Notch-IC), thereby activating Notch1 signaling selectively in this cell type.

Next, we examined whether Notch-IC over-expression, specifically in BMECs *in vivo*, would affect the diet-induced downregulation of Glut1 expression. Here, we compared Glut1 expression in BMECs of the PVH in littermate control (Ctrl) and NotchIC$^{BMECs}$ mice following 3 days of HFD feeding (Figure 3A). Congruent with previous studies, we observed a profound reduction in Glut1 protein expression in lectin-positive VECs after 3 days of HFD feeding in Ctrl mice (Figures 3A and 3B). In contrast, Glut1 expression in BMECs remained significantly higher in NotchIC$^{BMECs}$ mice at this time point (Figures 3A and

CellPress
OPEN ACCESS

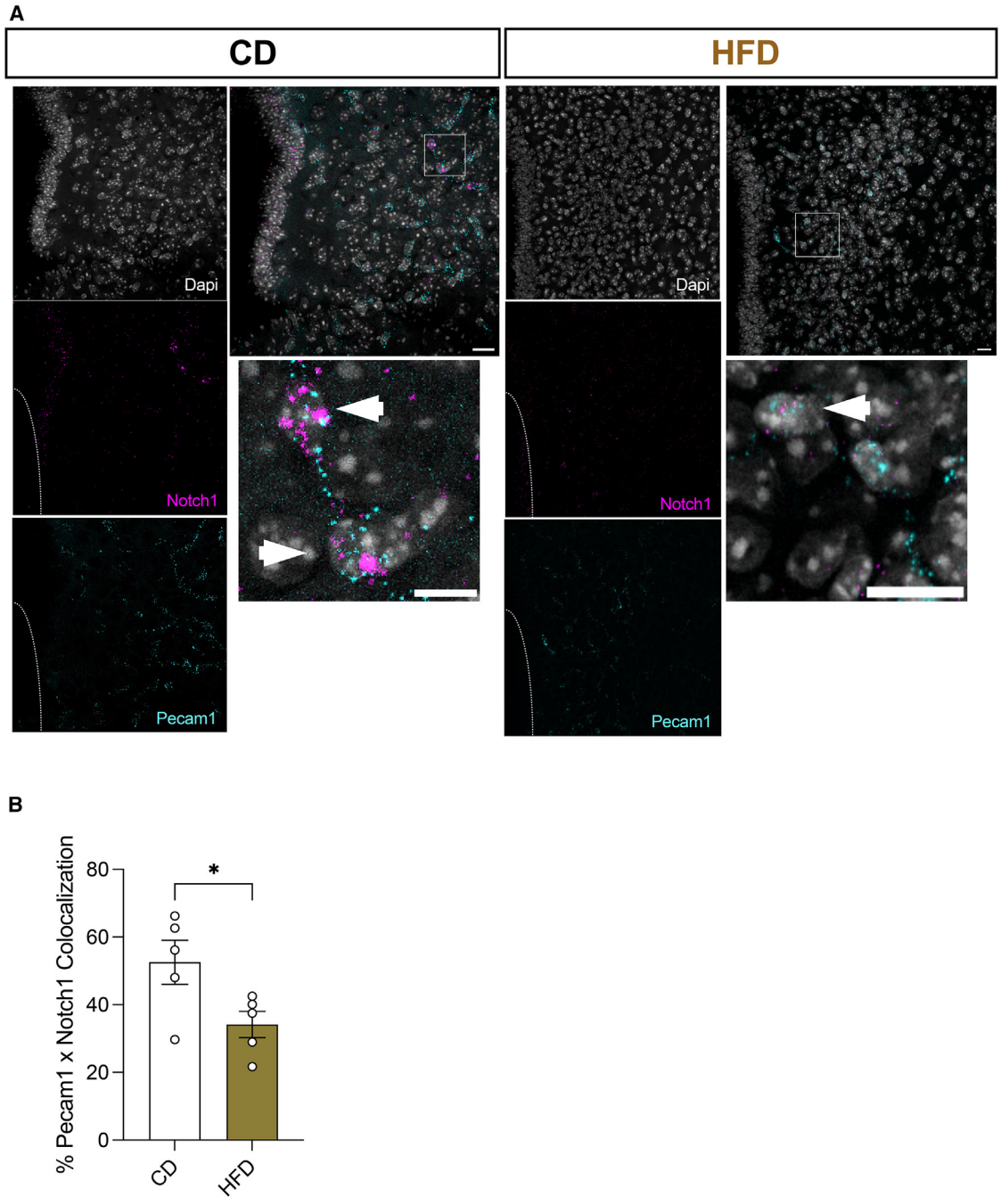


**Figure 1. *In situ* RNA analysis reveals Notch1 downregulation upon diet manipulation**

(A) Representative images of Pecam1 (cyan) and Notch1 (magenta) mRNA expression in the PVH. Scale bar, 20 μm.

(B) Quantification of Pecam1- and Notch1-positive BMECs in PVH. $n = 5$ mice per group. Results are presented as mean ± SEM. $^{*}p < 0.05$.

3B). As previously reported, upon prolonged HFD feeding, Glut1 expression in BMECs of Ctrl mice gradually increased and reached similar levels to those observed in NotchIC$^{BMECs}$ mice after 14 days of HFD feeding (Figure 3B). Similar dynamic changes of Glut1 expression were observed in the ARC of Ctrl and NotchIC$^{BMECs}$ mice upon HFD feeding (Figures S5A and S5B).

To determine the functional consequences of Notch1 overactivation on brain glucose uptake regulation upon HFD feeding *in vivo*, we next assessed brain glucose uptake in Ctrl and NotchIC$^{BMECs}$ mice via $^{18}$F-FDG positron emission tomography (PET) imaging. As expected, 3 days of HFD feeding resulted in a decrease of glucose uptake into the hypothalamus of Ctrl mice (Figures 3C and 3D). In contrast, 3 days of HFD feeding

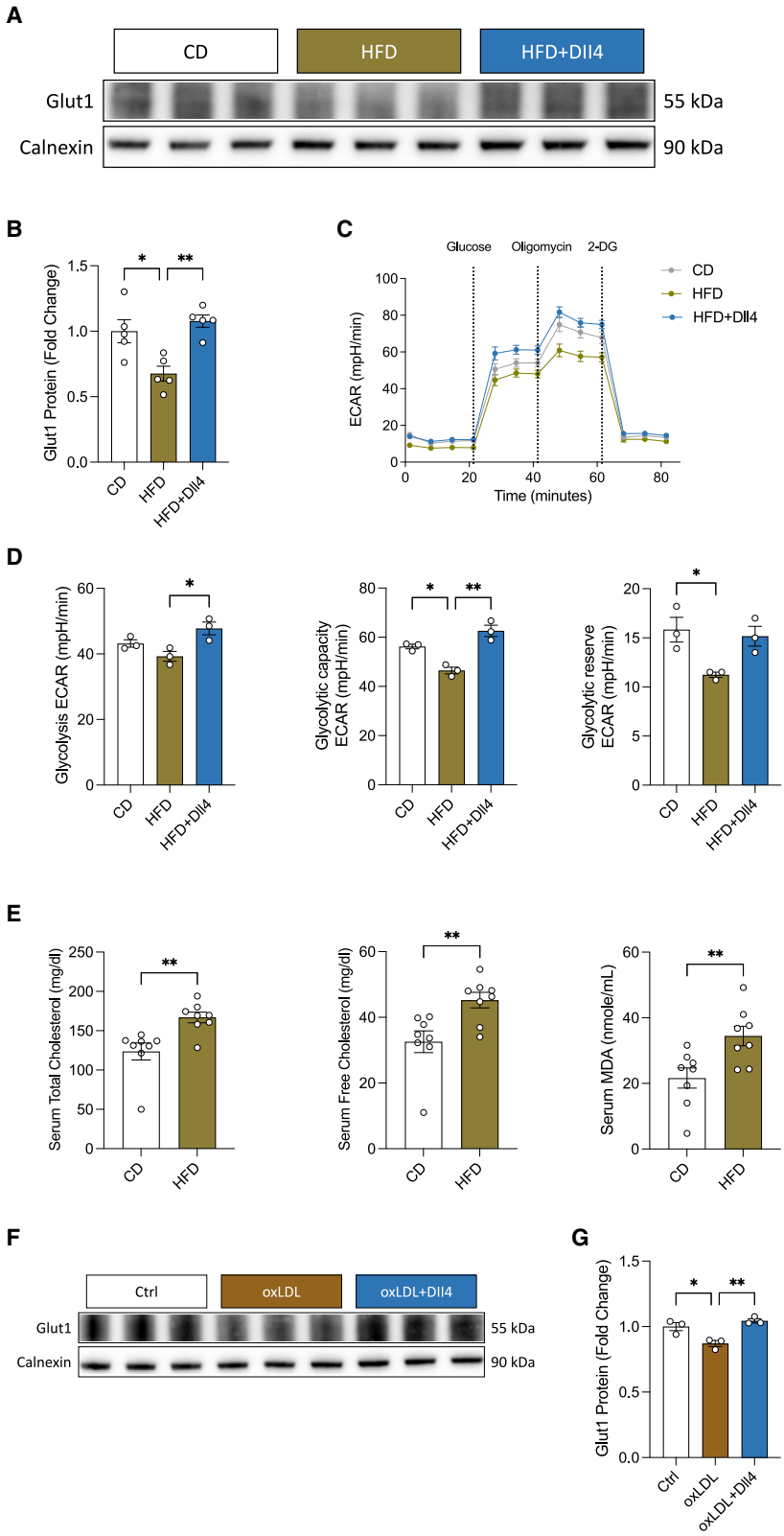


**Figure 2. Notch signaling regulates Glut1 expression *in vitro***

(A and B) Representative western blot analysis (A) and quantification (B) of Glut1 protein expression in cultured cEND cells. Cells were treated for 24 h with medium containing 10% serum derived from mice fed either a control diet (CD) for 3 days or a HFD for 3 days or from HFD-fed mice with recombinant Dll4 (1 μg/mL) added to the serum prior to incubation. Each lane represents lysates of cEND cells, which had been incubated with a pooled serum of different CD- or HFD-fed mice. $n = 5$ biological replicates.

(C and D) Representative analysis (C) and quantification (D) of glycolytic flux in cultured cEND cells treated for 24 h with medium containing 10% serum obtained from mice fed either a CD for 3 days or a HFD for 3 days or from HFD-fed mice with recombinant Dll4 (1 μg/mL) added to the serum prior to incubation. cEND cells were incubated with pooled serum from multiple CD- or HFD-fed animals. $n = 3$ independent experiments.

(E) C57BL/6N wild-type mice were fed a CD or HFD for 3 days. Serum levels of total cholesterol, free cholesterol, and malondialdehyde (MDA) were measured. $n = 8$ mice per group.

(F and G) Representative western blot analysis (F) and quantification (G) of Glut1 protein expression in cultured cEND cells, which had been treated with oxLDL (20 μg/mL) for 24 h in the presence or absence of Dll4 (1 μg/mL). $n = 3$ biological replicates.

Results are presented as mean ± SEM. $^{*}p < 0.05$ and $^{**}p < 0.01$.

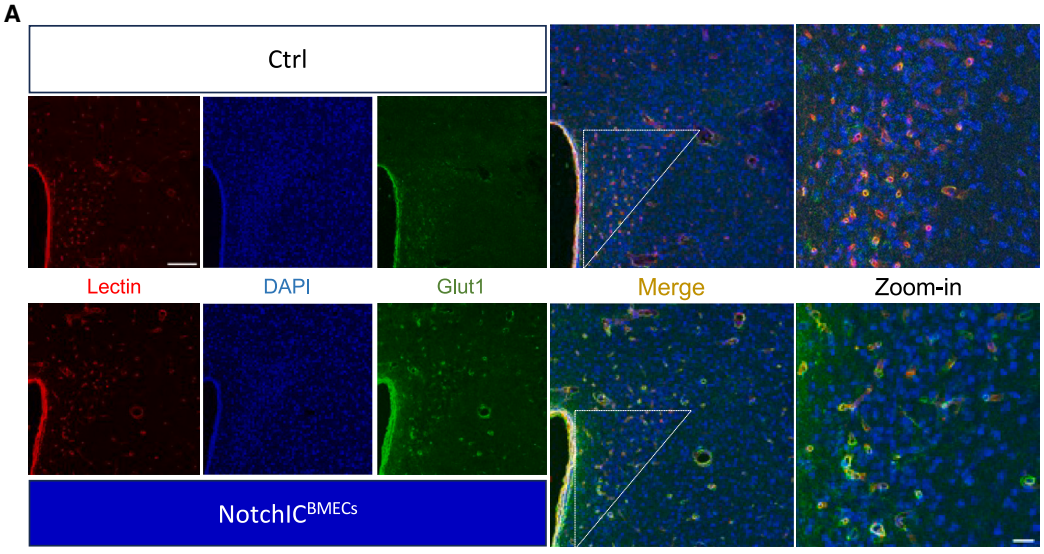


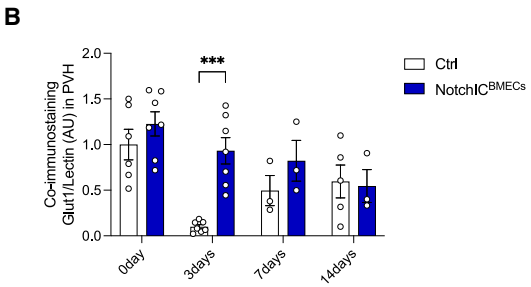


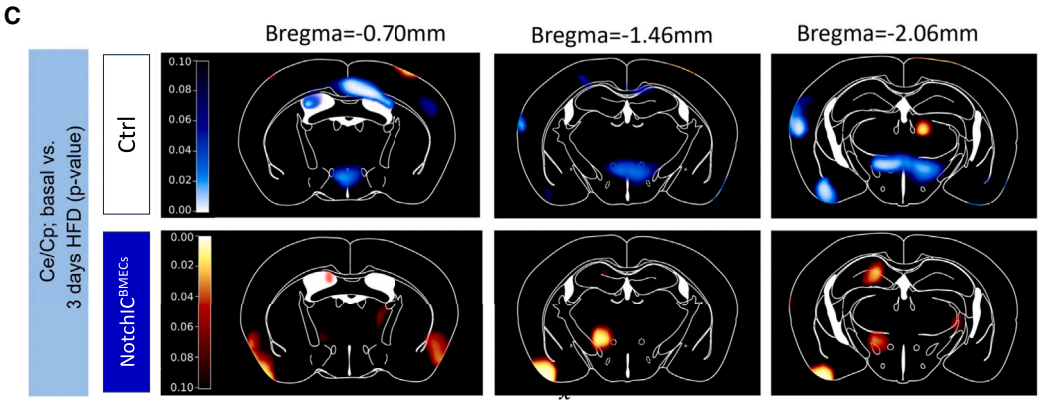


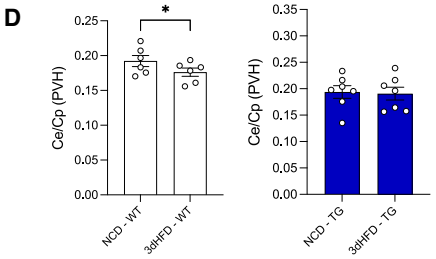


*(legend on next page)*

failed to alter hypothalamic glucose uptake in NotchIC$^{BMECs}$ mice (Figures 3C and 3D), while this reduction was no longer significant upon prolonged HFD feeding after 28 days (Figures S6A and S6B). Taken together, these data demonstrate that Notch activation in BMECs *in vivo* can surmount the downregulation of Glut1 expression and subsequent reduction of hypothalamic glucose uptake following a short-term nutritional insult. Additionally, *Notch* downregulation largely contributes to the diet-induced metabolic rewiring of BMECs *in vivo*.

## Short-term HFD feeding leads to altered caveola formation in BMECs and alters BBB permeability

In addition to the diet-induced downregulation of *Glut1* expression and the coordinated downregulation of Notch signaling components, bacTRAP ribosomal profiling of BMECs of HFD- vs. CD-fed animals revealed an upregulation of *Cav1* expression and gene networks related to membrane domain regulation (Figures 4A and 4B). Notably, previous studies have shown that Notch signaling regulates caveola formation and function in retinal endothelial cells.[14] Therefore, we next aimed to compare caveola formation on BMECs of animals exposed to CD or HFD feeding. To complement this study regarding the potential role of Notch signaling in BMECs caveola formation, we also analyzed caveolae of Ctrl and NotchIC$^{BMECs}$ mice exposed to CD or HFD feeding for 3 days. Interestingly, HFD feeding increased the number of vesicular structures in BMECs of Ctrl mice but not NotchIC$^{BMECs}$ mice (Figures 4C and 4D). In addition to reduced Glut1 expression and hypothalamic glucose uptake, these data also indicate that Notch signaling regulates caveola formation in BMECs after 3 days of HFD feeding.

Since caveola formation has been critically linked to BBB permeability, we assessed the barrier function following a short-term nutritional transition. To this end, Ctrl and NotchIC$^{BMECs}$ mice exposed to CD or HFD feeding for 3 days were injected intravenously with 10 kD fluorescently labeled dextran. As evidenced by the assessment of dextran immunoreactivity in the vicinity of lectin-positive BBB vessels, we found an increase in leaky BBB vessels in Ctrl mice after 3 days of HFD feeding compared to animals on CD (Figures 4E and 4F). Conversely, increased HFD-induced BBB vessel leakiness was prevented in NotchIC$^{BMECs}$ mice (Figures 4E and 4F). These data indicate that Notch signaling in BMECs regulates not only brain glucose uptake but also diet-associated changes in BBB permeability.

Caveolin expression has been implicated in the control of insulin transport, as endothelial-cell-specific caveolin-deficient animals exhibit reduced insulin uptake in skeletal muscle.[9] We have recently demonstrated that insulin transport in the CNS requires insulin receptor expression in tanycytes but not BMECs.[6] Collectively, these data point to the possibility that efficient insulin transport into the CNS might require caveola-mediated transport across endothelial cells and presumably subsequent insulin-receptor-dependent regulation of transport in tanycytes. To address this, we next assessed the uptake of insulin into the mediobasal hypothalamus (MBH) through intravenous injection of fluorescently labeled insulin into Ctrl and NotchIC$^{BMECs}$ mice, which were exposed to CD or HFD feeding for 3 days. CD-fed NotchIC$^{BMECs}$ mice exhibited a trend toward reduced insulin uptake in the MBH compared to CD-fed Ctrl mice (Figures S7A and S7B). However, insulin uptake in the MBH was significantly reduced in HFD-fed NotchIC$^{BMECs}$ mice compared to HFD-fed Ctrl mice (Figures S7A and S7B). Since the fluorescently labeled insulin retains the same signaling capacity as regular insulin, we next investigated the activation of insulin-dependent AKT signaling in the MBH of NotchIC$^{BMECs}$ mice and Ctrl mice under different dietary conditions. CD-fed NotchIC$^{BMECs}$ mice displayed no alteration in insulin-evoked AKT phosphorylation (pAKT) relative to CD-fed Ctrl mice (Figures S7A and S7C). On the contrary, pAKT immunoreactivity was clearly reduced in the MBH of HFD-fed NotchIC$^{BMECs}$ mice compared to HFD-fed Ctrl mice (Figures S7A and S7C). In summary, the reduction of *Cav1* expression, concomitant with decreased caveola formation and BBB permeability, limited insulin access and action in the MBH of HFD-fed NotchIC$^{BMECs}$ mice. Notably, previous studies have described the critical role of insulin transport into the MBH[6] and insulin action in the agouti-related peptide (AgRP)-expressing neurons of the MBH[15–17] to control peripheral insulin sensitivity. We next performed systemic insulin sensitivity tests on NotchIC$^{BMECs}$ mice and Ctrl mice under different dietary conditions. Normal chow diet (NCD)-fed NotchIC$^{BMECs}$ mice and Ctrl mice showed similar basal blood glucose concentrations and insulin sensitivity (Figures S7D). However, NotchIC$^{BMECs}$ mice exhibited increased blood glucose concentrations before and after insulin injection after 3 days of HFD feeding compared to HFD-fed Ctrl mice (Figures S7E). Interestingly, these changes in glucose metabolism occurred in the absence of alterations in food intake, respiratory exchange ratio, or energy expenditure between Ctrl and NotchIC$^{BMECs}$ mice under either dietary condition (Figures S8A–S8I). Collectively, these data indicate that Notch activation limits insulin transport and action in the MBH, which resulted in impaired systemic insulin sensitivity upon short-term HFD feeding.

**Figure 3. Notch signaling regulates Glut1 expression *in vivo***

(A) Representative images of Glut1 (red) and lectin-positive capillaries (green) in control (Ctrl) and NotchIC$^{BMECs}$ mice upon 3 days of HFD feeding on PVH brain sections. Scale bar, 100 μm.

(B) Quantification of co-immunostaining of Glut1 and lectin on PVH brain sections. $n = 6$ Ctrl and $n = 7$ NotchIC$^{BMECs}$ mice on NCD condition; $n = 7$ Ctrl mice and $n = 7$ NotchIC$^{BMECs}$ mice on 3 days of HFD feeding condition; $n = 3$ Ctrl mice and $n = 3$ NotchIC$^{BMECs}$ mice on 7 days of HFD feeding condition; and $n = 5$ Ctrl mice and $n = 3$ NotchIC$^{BMECs}$ mice on 14 days of HFD feeding condition.

(C) PET-computed tomography (CT) images showing differential regional glucose uptake in Ctrl and NotchIC$^{BMECs}$ mice before and 3 days after HFD exposure. Color code represents the $p$ value for the indicated voxels in a paired Student's t test before and after the HFD switch. Decreases in glucose uptake are shown in the blue color and increases in glucose uptake are shown in the yellow color. $n = 6$ Ctrl and $n = 7$ NotchIC$^{BMECs}$ mice.

(D) Quantification of brain glucose uptake before and 3 days after HFD exposure in the PVH. $n = 6$ Ctrl and $n = 7$ NotchIC$^{BMECs}$ mice.

Data were analyzed using a paired Student's t test. Results are presented as mean ± SEM. $^{*}p < 0.05$ and $^{***}p < 0.001$.

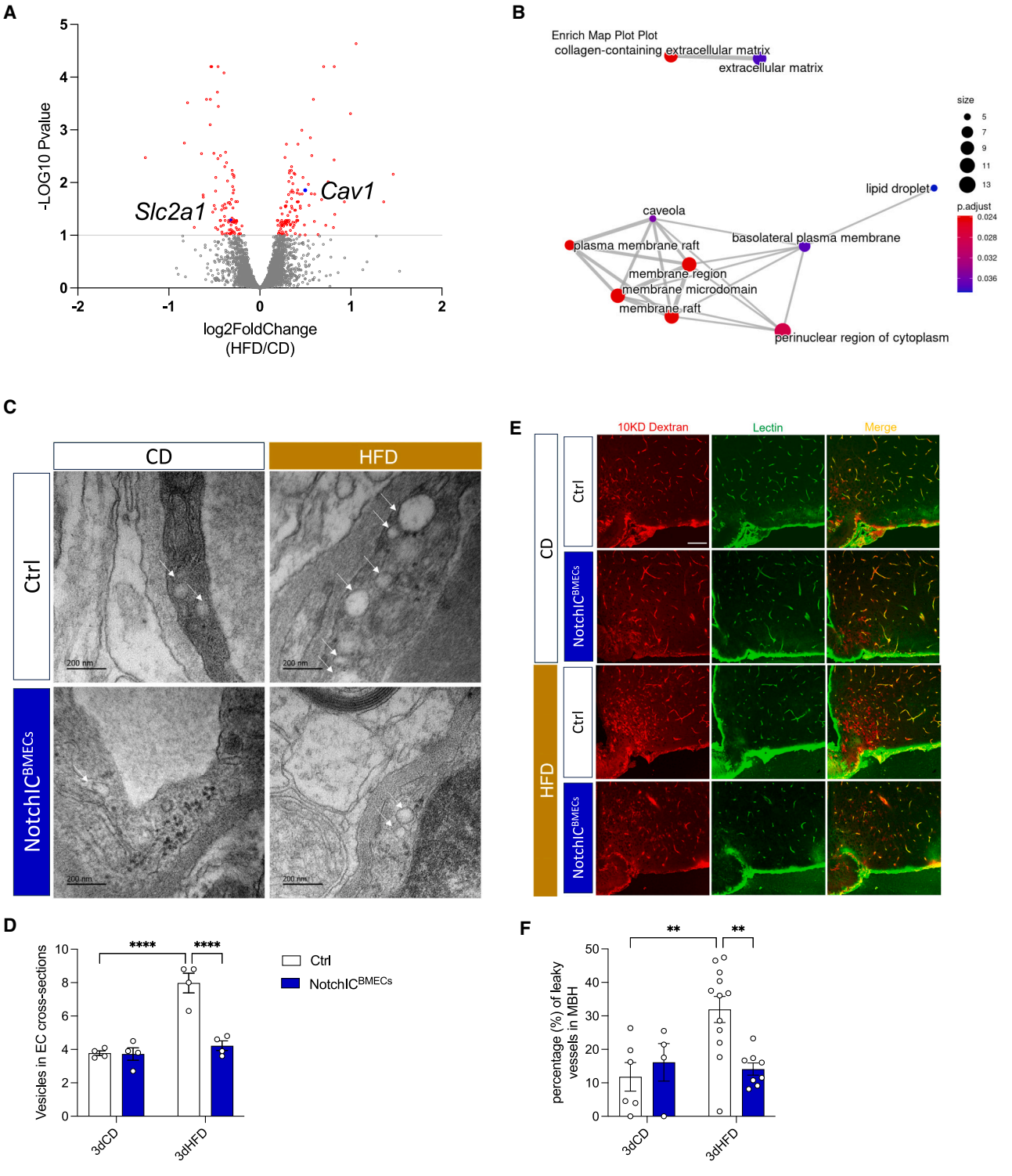


**Figure 4. Notch1 activation in BMECs decreases BBB permeability in the MBH**

(A) bacTRAP-based RNA-seq profiling of hypothalamic tissue of Slco1c1CreERT2$^{tg/wt}$:ROSA26lSlL10aGFP$^{tg/wt}$ mice fed with 3 days of CD or HFD.

(B) Gene Ontology (GO) term analysis of enriched transcripts in BMECs of HFD-fed animals. Adjusted *p* values for each significantly enriched pathway are shown.

(C and D) Representative TEM (transmission electron microscope) images (C) and quantification (D) of hypothalamic EC vesicles (white arrows) in Ctrl and NotchIC$^{BMECs}$ mice on 3 days of CD or HFD feeding condition. *n* = 4 mice per group. Ctrl mice on CD condition: 87 sections were analyzed, Ctrl mice on HFD

*(legend continued on next page)*

## DISCUSSION

Tight and coordinated regulation of BBB integrity is of critical importance for regulating hormone and nutrient access into the CNS. We have previously shown that short-term HFD feeding (3 days) fundamentally reduces hypothalamic glucose uptake via the downregulation of BMEC Glut1 expression.[1]

Here, we describe that HFD-induced downregulation of *Glut1* is preceded by Notch inhibition *in vivo*. Moreover, Notch activation can overcome the HFD-fed mouse serum-induced reduction in Glut1 expression and glycolysis *in vitro*, as well as surmount HFD-feeding-induced suppression of Glut1 expression in BMECs and hypothalamic glucose uptake *in vivo*. These findings complement a recent study showing that Notch activation induces Glut1 expression in cultured endothelial cells.[18] We provide further evidence that, at least *in vitro*, oxLDL, which readily increases in the serum of HFD-fed mice, can suppress Glut1 expression in cultured endothelial cells. In fact, a previous study has demonstrated oxLDL-induced angiogenesis in HUVECs via Notch suppression.[13] Nevertheless, we cannot exclude the possibility of other mediators in the circulation of HFD-fed mice, which may contribute to diet-induced Notch inhibition in BMECs.

The present study uncovers a profound induction of BMEC Cav1 expression upon short-term HFD feeding and subsequent Notch inhibition. Furthermore, we showed that Notch activation can suppress the HFD-induced Cav1 expression and excessive vesicle formation *in vivo*. This further supports the notion that Notch inhibition upon short-term HFD feeding not only decreased Glut1 expression but also increased Cav1 expression. Functionally, we can link the HFD-induced, Notch-dependent regulation of Cav1 to altered BBB permeability and hypothalamic insulin transport and action. These findings are consistent with previous studies showing that antibody and genetic inactivation of Dll4 or Notch enhances endothelial transcytosis, which results in hyperpermeability of the blood-retinal barrier.[14] Interestingly, Cav1 has been identified as a critical factor for vascular endothelial insulin uptake, and this mechanism is impaired in HFD-fed mice.[19,20] Of note, endothelial Notch signaling controls endothelial insulin transport in the skeletal muscle.[9] Conversely, insulin uptake and transcytosis appear to be clathrin dependent in cultured human adipose microvascular cells since these processes remain unaffected by Cav1 knockdown.[21] Nevertheless, our data indicate that reduced hypothalamic insulin uptake and action upon Notch activation and Cav1 suppression in BMECs argue for a potential role of Cav1-dependent insulin transcytosis in this cell type. These findings add to the long-standing question of how insulin enters the CNS. While it has been proposed that insulin-receptor-mediated transcytosis in vascular endothelial cells may contribute to this process,[5] recent studies have unveiled that insulin uptake and action in the hypothalamus remain unaffected by endothelial-cell-specific insulin receptor knockout but depend on insulin receptor expression in tanycytes.[6,7] Our previous work has demonstrated that insulin action in the CNS, particularly in AgRP-expressing neurons in the ARC, is required for proper control of systemic insulin sensitivity via hepatic glucose production and brown adipose tissue glucose uptake.[15–17,22,23] Thus, impaired insulin access and action in the ARC of HFD-fed NotchIC$^{BMECs}$ mice indicates that HFD-induced Notch suppression and the subsequent increase of Cav1 expression contribute to the maintenance of systemic insulin sensitivity after short-term HFD feeding.

### Limitations of the study

While we have detected parallel changes of Notch1 and Glut1 downregulation both in the ARC and the PVH upon short-term HFD feeding, the investigation of changes in relation to caveola formation, BBB permeability, and insulin signaling have been limited to analyses in the ARC. Furthermore, future studies are necessary to establish the exact molecular mechanism(s) of Notch-dependent regulation of Glut1 in order to further delineate the mechanisms through which high fat suppresses endothelial Notch signaling. Moreover, our study does not address how factors other than BMEC Glut1 regulation and functionality may contribute to altered brain glucose uptake during dietary transitions.

## RESOURCE AVAILABILITY

### Lead contact

Further information and requests for resources and reagents should be directed to and will be fulfilled by the lead contact, Jens C. Brüning (bruening@sf.mpg.de).

### Materials availability

No unique reagents were generated in this study.

### Data and code availability

RNA sequencing data are deposited in the NCBI Gene Expression Omnibus, all original images of immunohistochemistry and electron microscopy (EM) are deposited at Mendeley Data, and all are publicly available as of the date of publication. Accession numbers are listed in the key resources table.

No code was uniquely generated.

## ACKNOWLEDGMENTS

We thank Christiane Schäfer, Cordula Schäfer, Jens Alber, Pia Scholl, Nadine Spenrath, and Christian Heilinger for excellent technical support. We are grateful to Dr. Janine Altmüller, Dr. Kerstin Becker, and Marek Franitza for their support in RNA sequencing experiments (Cologne Center for Genomics, University of Cologne, Germany). We thank Dr. Astrid Schauss and Janine Heise from the CECAD imaging facility for EM support. The authors wish to thank Markus Schwaninger for providing the Slcoc1CreERT2 transgenic mice used in this study. This project has received funding from the European Research Council (ERC) under the European Union's Horizon 2020 research and innovation programme (grant agreement no. 742106) to J.C.B., the BMBF through the German Center for Diabetes Research (DZD) to J.C.B., and through the CMMC to J.C.B. Y.Z. acknowledges support from China

condition: 73 sections were analyzed, NotchIC$^{BMECs}$ mice on CD condition: 92 sections were analyzed, and NotchIC$^{BMECs}$ mice on HFD condition: 80 sections were analyzed. Scale bar, 200 nm.

(E and F) Representative confocal microscopy analysis of extravascular 10 kDa Tetramethylrhodamine-dextran tracer (E) and quantification (F) of the percentage of leaky vessels in MBH brain sections of Ctrl and NotchIC$^{BMECs}$ mice on 3 days of CD ($n$ = 6/4) or HFD ($n$ = 12/8) feeding condition. Scale bar, 100 μm. Results are presented as mean ± SEM. $^{**}p < 0.01$ and $^{***}p < 0.001$.

Scholarship Council (CSC), China. A.J. received funding from Helmholtz Center Munich and the federal government of Saxony, Germany.

## AUTHOR CONTRIBUTIONS

Conceptualization, A.J. and J.C.B.; methodology, Y.Z., R.J., M.P.; investigation, Y.Z., O.M., A.J., H.K., A.L.C., R.J., P.K., and L.S.; formal analysis, Y.Z., O.M., R.J., P.K., and L.S.; visualization, Y.Z., O.M., H.B., and A.L.C.; writing – original draft, J.C.B.; writing – review & editing, Y.Z., W.C., A.J., and J.C.B.; project administration, Y.Z., A.J., and J.C.B.; resources, F.T.W., and J.C.B.

## DECLARATION OF INTERESTS

J.C.B. is co-founder of Cerapeutix and has received research funding through collaborations with Sanofi Aventis and Novo Nordisk, Inc., and he also consulted for Eli Lilly and Company and Novo Nordisk, all of which did not affect the content of this article.

## STAR★METHODS

Detailed methods are provided in the online version of this paper and include the following:

- KEY RESOURCES TABLE
- EXPERIMENTAL MODEL AND STUDY PARTICIPANT DETAILS
  - Animal care
  - Mice and manipulations
  - Cell lines
- METHOD DETAILS
  - bacTRAP-based ribosomal profiling of hypothalamic ECs
  - RNA bulk sequencing
  - *In situ* hybridization
  - Western blotting
  - Measurement of glycolytic flux
  - Analysis of mouse serum
  - Immunohistochemistry
  - Positron emission tomography (PET) scanning
  - Electron microscopy imaging
  - Blood-brain barrier permeability assay
  - Fluorescently labeled insulin injection and imaging
  - Intraperitoneal insulin tolerance test
  - Indirect calorimetry
- QUANTIFICATION AND STATISTICAL ANALYSIS

## SUPPLEMENTAL INFORMATION

Supplemental information can be found online at https://doi.org/10.1016/j.celrep.2025.115522.

Received: November 22, 2023
Revised: July 28, 2024
Accepted: March 14, 2025
Published: April 3, 2025

## REFERENCES

1. Jais, A., Solas, M., Backes, H., Chaurasia, B., Kleinridders, A., Theurich, S., Mauer, J., Steculorum, S.M., Hampel, B., Goldau, J., et al. (2016). Myeloid-Cell-Derived VEGF Maintains Brain Glucose Uptake and Limits Cognitive Impairment in Obesity. Cell *165*, 882–895. https://doi.org/10.1016/j.cell.2016.03.033.
2. Ogata, S., Ito, S., Masuda, T., and Ohtsuki, S. (2019). Changes of Blood-Brain Barrier and Brain Parenchymal Protein Expression Levels of Mice under Different Insulin-Resistance Conditions Induced by High-Fat Diet. Pharm. Res. *36*, 141. https://doi.org/10.1007/s11095-019-2674-8.
3. Banks, W.A., Jaspan, J.B., and Kastin, A.J. (1997). Selective, physiological transport of insulin across the blood-brain barrier: novel demonstration by species-specific radioimmunoassays. Peptides *18*, 1257–1262. https://doi.org/10.1016/s0196-9781(97)00198-8.
4. Banks, W.A., Kastin, A.J., Huang, W., Jaspan, J.B., and Maness, L.M. (1996). Leptin enters the brain by a saturable system independent of insulin. Peptides *17*, 305–311. https://doi.org/10.1016/0196-9781(96)00025-3.
5. Konishi, M., Sakaguchi, M., Lockhart, S.M., Cai, W., Li, M.E., Homan, E.P., Rask-Madsen, C., and Kahn, C.R. (2017). Endothelial insulin receptors differentially control insulin signaling kinetics in peripheral tissues and brain of mice. Proc. Natl. Acad. Sci. USA *114*, E8478–E8487. https://doi.org/10.1073/pnas.1710625114.
6. Porniece Kumar, M., Cremer, A.L., Klemm, P., Steuernagel, L., Sundaram, S., Jais, A., Hausen, A.C., Tao, J., Secher, A., Pedersen, T.Å., et al. (2021). Insulin signalling in tanycytes gates hypothalamic insulin uptake and regulation of AgRP neuron activity. Nat. Metab. *3*, 1662–1679. https://doi.org/10.1038/s42255-021-00499-0.
7. Rhea, E.M., Rask-Madsen, C., and Banks, W.A. (2018). Insulin transport across the blood-brain barrier can occur independently of the insulin receptor. J. Physiol. *596*, 4753–4765. https://doi.org/10.1113/JP276149.
8. Garcia-Caceres, C., Quarta, C., Varela, L., Gao, Y., Gruber, T., Legutko, B., Jastroch, M., Johansson, P., Ninkovic, J., Yi, C.X., et al. (2016). Astrocytic Insulin Signaling Couples Brain Glucose Uptake with Nutrient Availability. Cell *166*, 867–880. https://doi.org/10.1016/j.cell.2016.07.028.
9. Hasan, S.S., Jabs, M., Taylor, J., Wiedmann, L., Leibing, T., Nordström, V., Federico, G., Roma, L.P., Carlein, C., Wolff, G., et al. (2020). Endothelial Notch signaling controls insulin transport in muscle. EMBO Mol. Med. *12*, e09271. https://doi.org/10.15252/emmm.201809271.
10. Briot, A., Civelek, M., Seki, A., Hoi, K., Mack, J.J., Lee, S.D., Kim, J., Hong, C., Yu, J., Fishbein, G.A., et al. (2015). Endothelial NOTCH1 is suppressed by circulating lipids and antagonizes inflammation during atherosclerosis. J. Exp. Med. *212*, 2147–2163. https://doi.org/10.1084/jem.20150603.
11. Ridder, D.A., Lang, M.F., Salinin, S., Röderer, J.P., Struss, M., Maser-Gluth, C., and Schwaninger, M. (2011). TAK1 in brain endothelial cells mediates fever and lethargy. J. Exp. Med. *208*, 2615–2623. https://doi.org/10.1084/jem.20110398.
12. Liu, Y., Cao, Y., Zhang, W., Bergmeier, S., Qian, Y., Akbar, H., Colvin, R., Ding, J., Tong, L., Wu, S., et al. (2012). A small-molecule inhibitor of glucose transporter 1 downregulates glycolysis, induces cell-cycle arrest, and inhibits cancer cell growth in vitro and in vivo. Mol. Cancer Ther. *11*, 1672–1682. https://doi.org/10.1158/1535-7163.MCT-12-0131.
13. Yin, J., Huang, F., Yi, Y., Yin, L., and Peng, D. (2016). EGCG attenuates atherosclerosis through the Jagged-1/Notch pathway. Int. J. Mol. Med. *37*, 398–406. https://doi.org/10.3892/ijmm.2015.2422.
14. Yang, J.M., Park, C.S., Kim, S.H., Noh, T.W., Kim, J.H., Park, S., Lee, J., Park, J.R., Yoo, D., Jung, H.H., et al. (2020). Dll4 Suppresses Transcytosis for Arterial Blood-Retinal Barrier Homeostasis. Circ. Res. *126*, 767–783. https://doi.org/10.1161/CIRCRESAHA.119.316476.
15. Konner, A.C., Janoschek, R., Plum, L., Jordan, S.D., Rother, E., Ma, X., Xu, C., Enriori, P., Hampel, B., Barsh, G.S., et al. (2007). Insulin action in AgRP-expressing neurons is required for suppression of hepatic glucose production. Cell Metab. *5*, 438–449. https://doi.org/10.1016/j.cmet.2007.05.004.
16. Dodd, G.T., Lee-Young, R.S., Brüning, J.C., and Tiganis, T. (2018). TCPTP Regulates Insulin Signaling in AgRP Neurons to Coordinate Glucose Metabolism With Feeding. Diabetes *67*, 1246–1257. https://doi.org/10.2337/db17-1485.
17. Dodd, G.T., Kim, S.J., Méquinion, M., Xirouchaki, C.E., Brüning, J.C., Andrews, Z.B., and Tiganis, T. (2021). Insulin signaling in AgRP neurons regulates meal size to limit glucose excursions and insulin resistance. Sci. Adv. *26*, 9, Print 2021 Feb. https://doi.org/10.1126/sciadv.abf4100.
18. Veys, K., Fan, Z., Ghobrial, M., Bouché, A., García-Caballero, M., Vriens, K., Conchinha, N.V., Seuwen, A., Schlegel, F., Gorski, T., et al. (2020). Role of the GLUT1 Glucose Transporter in Postnatal CNS Angiogenesis

and Blood-Brain Barrier Integrity. Circ. Res. *127*, 466–482. https://doi.org/10.1161/CIRCRESAHA.119.316463.

19. Wang, H., Wang, A.X., Aylor, K., and Barrett, E.J. (2015). Caveolin-1 phosphorylation regulates vascular endothelial insulin uptake and is impaired by insulin resistance in rats. Diabetologia *58*, 1344–1353. https://doi.org/10.1007/s00125-015-3546-3.

20. Wang, H., Wang, A.X., and Barrett, E.J. (2011). Caveolin-1 is required for vascular endothelial insulin uptake. Am. J. Physiol. Endocrinol. Metab. *300*, E134–E144. https://doi.org/10.1152/ajpendo.00498.2010.

21. Azizi, P.M., Zyla, R.E., Guan, S., Wang, C., Liu, J., Bolz, S.S., Heit, B., Klip, A., and Lee, W.L. (2015). Clathrin-dependent entry and vesicle-mediated exocytosis define insulin transcytosis across microvascular endothelial cells. Mol. Biol. Cell *26*, 740–750. https://doi.org/10.1091/mbc.E14-08-1307.

22. Brüning, J.C., Gautam, D., Burks, D.J., Gillette, J., Schubert, M., Orban, P.C., Klein, R., Krone, W., Müller-Wieland, D., and Kahn, C.R. (2000). Role of brain insulin receptor in control of body weight and reproduction. Science *289*, 2122–2125. https://doi.org/10.1126/science.289.5487.2122.

23. Steculorum, S.M., Ruud, J., Karakasilioti, I., Backes, H., Engström Ruud, L., Timper, K., Hess, M.E., Tsaousidou, E., Mauer, J., Vogt, M.C., et al. (2016). AgRP Neurons Control Systemic Insulin Sensitivity via Myostatin Expression in Brown Adipose Tissue. Cell *165*, 125–138. https://doi.org/10.1016/j.cell.2016.02.044.

24. Forster, C., Silwedel, C., Golenhofen, N., Burek, M., Kietz, S., Mankertz, J., and Drenckhahn, D. (2005). Occludin as direct target for glucocorticoid-induced improvement of blood-brain barrier properties in a murine in vitro system. J. Physiol. *565*, 475–486. https://doi.org/10.1113/jphysiol.2005.084038.

25. Biglari, N., Gaziano, I., Schumacher, J., Radermacher, J., Paeger, L., Klemm, P., Chen, W., Corneliussen, S., Wunderlich, C.M., Sue, M., et al. (2021). Functionally distinct POMC-expressing neuron subpopulations in hypothalamus revealed by intersectional targeting. Nat. Neurosci. *24*, 913–929. https://doi.org/10.1038/s41593-021-00854-0.

26. Heiman, M., Schaefer, A., Gong, S., Peterson, J.D., Day, M., Ramsey, K.E., Suárez-Fariñas, M., Schwarz, C., Stephan, D.A., Surmeier, D.J., et al. (2008). A translational profiling approach for the molecular characterization of CNS cell types. Cell *135*, 738–748. https://doi.org/10.1016/j.cell.2008.10.028.

27. Heiman, M., Kulicke, R., Fenster, R.J., Greengard, P., and Heintz, N. (2014). Cell type-specific mRNA purification by translating ribosome affinity purification (TRAP). Nat. Protoc. *9*, 1282–1291. https://doi.org/10.1038/nprot.2014.085.

28. Yates, A., Beal, K., Keenan, S., McLaren, W., Pignatelli, M., Ritchie, G.R.S., Ruffier, M., Taylor, K., Vullo, A., and Flicek, P. (2015). The Ensembl REST API: Ensembl Data for Any Language. Bioinformatics *31*, 143–145. https://doi.org/10.1093/bioinformatics/btu613.

29. Ewels, P., Hammarén, R., Peltzer, A., Moreno, D., Garcia, M., rfenouil, marchoeppner, et al. (2019). nf-core/rnaseq: nf-core/rnaseq version 1.4 "Gray Crocus Dachshund. Zenodo. https://doi.org/10.5281/zenodo.3490660.

30. Patro, R., Duggal, G., Love, M.I., Irizarry, R.A., and Kingsford, C. (2017). Salmon provides fast and bias-aware quantification of transcript expression. Nat. Methods *14*, 417–419. https://doi.org/10.1038/nmeth.4197.

31. Love, M.I., Huber, W., and Anders, S. (2014). Moderated estimation of fold change and dispersion for RNA-seq data with DESeq2. Genome Biol. *15*, 550. https://doi.org/10.1186/s13059-014-0550-8.

32. Cizek, J., Herholz, K., Vollmar, S., Schrader, R., Klein, J., and Heiss, W.D. (2004). Fast and robust registration of PET and MR images of human brain. Neuroimage *22*, 434–442. https://doi.org/10.1016/j.neuroimage.2004.01.016.

33. Paxinos, and G.F.K.B.J (2013). Paxinos and Franklin's the Mouse Brain in Stereotaxic Coordinates (Elsevier/AP).

34. Green, L.A., Gambhir, S.S., Srinivasan, A., Banerjee, P.K., Hoh, C.K., Cherry, S.R., Sharfstein, S., Barrio, J.R., Herschman, H.R., and Phelps, M.E. (1998). Noninvasive Methods for Quantitating Blood Time-Activity Curves from Mouse PET Images Obtained with Fluorine-18-Fluorodeoxyglucose. JNM (J. Nucl. Med.) *39*, 729–734.

## STAR★METHODS

### KEY RESOURCES TABLE

| REAGENT or RESOURCE | SOURCE | IDENTIFIER |
|---|---|---|
| Antibodies | | |
| Anti-GLUT1 | Merck Millipore | Cat# 07-1401; RRID:AB_1587074 |
| Anti-Calnexin | Merck Millipore | Cat# 208880; RRID:AB_2069031 |
| Alexa Fluor 488 goat anti-rabbit | Abcam | Cat# A11008; RRID:AB_143165 |
| Alexa Fluor 488 | Thermo Fisher Scientific | Cat# A11094; RRID:AB_221544 |
| Alexa 594 | Thermo Fisher Scientific | Cat# A21207; RRID:AB_141637 |
| DAPI | Thermo Fisher Scientific | Cat# 62248 |
| HRP-labelled anti-rabbit-IgG | Perkin Elmer | Cat# NEF812E001EA |
| Antibody GFP-19C8 | Memorial Sloan Kettering Monoclonal Antibody Facility | Cat# Htz-GFP-19F7; RRID: AB_2716736 |
| Antibody GFP-19F7 | Memorial Sloan Kettering Monoclonal Antibody Facility | Cat# Htz-GFP-19C8; RRID: AB_2716737 |
| Recombinant mouse Dll4 protein | R&D | Cat# 1389-D4 |
| Chemicals, peptides, and recombinant proteins | | |
| Tris Base | Sigma Aldrich | CAS# 77-86-1 |
| EDTA | Sigma Aldrich | Cat# E6758 |
| PMSF | AppliChem | Cat# A0999 |
| NAF | Sigma Aldrich | Cat# S7920 |
| cOmplete™, Mini Protease Inhibitor Cocktail | Roche | Cat# 11836153001 |
| PhosSTOP™, phosphatase inhibitor | Roche | Cat# 4906837001 |
| Western Blocking Reagent, Solution | Roche | Cat# 11921681001 |
| SignalStain® Antibody Diluent | Cell-Signaling Technology | Cat# 8112L |
| Sucrose | Sigma Aldrich | CAS# 57-50-1 |
| Paraformaldehyde | Sigma Aldrich | CAS# 30525-89-4 |
| 4x Laemmli sample buffer | Bio-Rad | Cat# 161-0747 |
| Tween® 20 (Polysorbate) | VWR France | CAS# 9005-64-5 |
| β-Mercaptoethanol | Sigma Aldrich | Cat# M3148 |
| HEPES | Sigma Aldrich | CAS# 7365-45-9 |
| Tamoxifen | Sigma Aldrich | Cat# T5648 |
| Human Insulin (Huminsulin Normal 100) | Lilly | Cat# HI0219 |
| Peanut Oil | Sigma Aldrich | Cat# P2144 |
| Feeding Needle | Fine Science Tools | Cat# 18061 |
| Blocking Reagent | Perkin Elmer | Cat# FP1020 |
| Gelatin | Merck | Cat# G1393 |
| DMEM | Thermo Fisher Scientific | Cat# 1960044 |
| Fetal Bovine Serum (FBS) | PAN Biotech | Cat# P30-3302 |
| L-Glutamine, 1% penicillin/streptomycin | Thermo Fisher Scientific | Cat# 15140-122 |
| AF488-labelled insulin | Novo Nordisk | N/A |
| Dextran, Tetramethylrhodamine (TMR) | Thermo Fisher Scientific | Cat# D1817 |
| Lycopersicon esculentum (Tomato) Lectin (LEL, TL), Fluorescein | Vector Biolabs | Cat# FL-1171-1 |
| NaCl | Merck | Cat# 1.06400 |
| NP-40 | Thermo Fisher Scientific | Cat# 85124 |
| Sodium-deoxycholate | Merck | Cat# 264103 |
| SDS | Merck | Cat# 11667289001 |
| Tris-HCL | Merck | Cat# 108315 |

(*Continued on next page*)

*Continued*

| REAGENT or RESOURCE | SOURCE | IDENTIFIER |
|---|---|---|
| DTT | Merck | Cat# DTT-RO |
| NuPAGE MOPS SDS | Thermo Fisher Scientific | Cat# NP0001 |
| Nonfat dried milk powder | PanReac AppliChem | Cat# A0830,0500 |
| TNB buffer | Cell Signaling | Cat# 4060 |
| Glycin | Invitrogen | Cat# 15527013 |
| Stainless-steel brain matrix | Agnthos | Cat# 69-2275-1 |
| $MgCl_2$ | Sigma Aldrich | Cat# 20833 |
| KCl | Sigma Aldrich | Cat# 58221 |
| Cyclohexamide | Sigma Aldrich | Cat# 18079 |
| Ribonuclease Inhibitor (RNAsin) | Promega | Cat# N2511 |
| Microcentrifuge tubes (RNase-free tubes, 1.5 mL) | Invitrogen | Cat# 3461 |
| **Critical commercial assays** | | |
| KAPA Library Quantification Kit | Sigma Aldrich | Cat# KK7100 |
| Lipid Peroxidation (MDA) Assay Kit | Sigma Aldrich | Cat# MAK085 |
| Cholesterol Quantification Kit | Sigma Aldrich | Cat# MAK043 |
| mirVana™ miRNA Isolation Kit | Invitrogen | Cat# AM1561 |
| Pierce™ BCA Protein Assay Kit | Thermo Fisher Scientific | Cat# 23225 |
| Seahorse XF Glycolysis Stress Test Kit | Agilent | Cat# 103020-100 |
| Rneasy Micro kit | Qiagen | Cat# 74004 |
| ACD HybEz hybridization system | ACD | Cat# 321642 |
| RNAscope Fluorescent Multiplex Detection Reagents v2 | ACD | Cat# 323100 |
| Probe Mm-Pecam1-C1 | ACD-RNAscope Probe | Cat# 316721 |
| Probe Mm-Notch1-C2 | ACD-RNAscope Probe | Cat# 404641 |
| Opal 520 Fluorophore | Akoya Bioscience | Cat# FP1487001KT |
| Opal 650 Fluorophore | Akoya Bioscience | Cat# FP1496001KT |
| **Deposited data** | | |
| RNAseq | This paper | NCBI GEO: GSE210620 |
| Imaging Data | This paper | Mendeley https://doi.org/10.17632/hsvw5jwtvz.1 |
| **Experimental models: Cell lines** | | |
| Brain (cerebral) capillary endothelial (cEND) cell line | | Förster et al.[24] |
| **Experimental models: Organisms/strains** | | |
| C57BL/6N | Charles River Laboratories | Strain# 027 |
| ROSA26lSIL10aGFP | Biglari et al.[25] | N/A |
| Gt(ROSA)26Sor$^{tm1(Notch1)Dam}$/J | Jackson Laboratory | Stock No. 008159 |
| NotchIC$^{BMECs}$ | This paper | N/A |
| Slco1c1-Cre$^{ERT2}$ | Ridder et al.[11] | N/A |
| **Software and algorithms** | | |
| Fiji/ImageJ software | (Schindelin et al. 2012) | https://imagej.net/software/fiji/ |
| GraphPad Prism (Version 9.1.0) | GraphPad Software Inc. | https://www.graphpad.com/scientific-software/prism/ |
| DigitalMicrograph | Gatan | Gatan Microscopy Suite Software \| Gatan, Inc. |
| BioRender | BioRender | www.biorender.com |
| **Other** | | |
| Control diet | ssniff Spezialdiäten GmbH | Cat# E15745-04 |
| High-fat diet | ssniff Spezialdiäten GmbH | Cat# E15742-34 |
| Mini Protein Gel | Invitrogen | Cat# NP00336box |
| Trans-Blot (R)Turbo, Midi Format, 0.2mm PVDF | Bio-Rad | Cat# 1704157 |

(*Continued on next page*)

*Continued*

| REAGENT or RESOURCE | SOURCE | IDENTIFIER |
|---|---|---|
| Epredia™ SuperFrost Ultra Plus™ GOLD Adhesion Slides | Thermo Fisher Scientific | Cat# 11976299 |
| Vectashield Antifade Mounting-Medium with DAPI | Vector Laboratories | Cat# H-1200 |
| Contour Blood Glucose Meter | Bayer HealthCare | N/A |
| Contour Next strips | Bayer HealthCare | Cat# #84167879 |
| Leica TCS SP-8-X Confocal microscope | Leica Microsystems | https://www.leica-microsystems.com/products/confocal-microscopes/p/leica-tcs-sp8-x/ |
| 2100 Bioanalyzer Instrument | Agilent Technologies | Part Number: G2939BA |
| FUSION Solo | Vilber Lourmat | http://www.vilber.de/produkte/chemilumineszenz/ |
| Seahorse XF96 Analyzer | Agilent Technologies | N/A |
| Phenomaster | TSE Systems | https://www.tse-systems.com/service/phenomaster/ |
| Camera OneView 4K 16bit | Gatan | N/A |
| Transmission Electron Microscope (JEOL JEM 2100Plus) | JEOL | N/A |
| Ultramicrotome | Leica Microsystems | EM-UC6 |
| Inveon preclinical PER/CT system | Siemens | N/A |
| Applied Biosystems 7900HT Sequence Detection | Thermo Fisher Scientific | N/A |
| Agilent 2200 TapeStation | Agilent | N/A |
| RNASeq System V2 | Tecan Life Sciences | N/A |
| Illumina NovaSeq S2 flowcell | Illumina | N/A |

## EXPERIMENTAL MODEL AND STUDY PARTICIPANT DETAILS

### Animal care

All animal procedures were conducted in compliance with protocols approved by the local authorities (Bezirksregierung Köln) and were in accordance with NIH guidelines. Mice were housed in individually ventilated cages at 22°C–24°C with 12 h light/dark cycle. Animals had *ad libitum* access to water and to a normal chow diet (NCD; V1554; Ssniff Diet) containing 67% of calories from carbohydrates, 23% calories from protein and 10% calories from fat, a control diet (CD; E15745-04, corresponds to D12450B; Ssniff Diet) containing 70% of calories from carbohydrates, 20% of calories from protein and 10% of calories from fat or a high fat-diet (HFD; E15742-34, corresponds to D12492; Ssniff Diet), containing 20% calories from carbohydrates, 20% calories from protein and 60% calories from fat. Food was only withdrawn if required for an experiment. Male mice are used for experiments, unless stated otherwise.

### Mice and manipulations

Mice carrying a loxP-flanked EGFP-RpL10a (annotated ROSA26lSIL10aGFP) were described elsewhere.[25] ROSA26lSIL10aGFP mice were crossed with Slco1c1-CreERT2 mice[11] to express a fusion protein of the ribosomal L10a protein with EGFP(L10a-EGFP) selectively in BMECs.

The Gt(ROSA)26Sor$^{tm1(Notch1)Dam/J}$ mouse strain was purchased from Jackson Laboratory (Stock No. 008159), these mice were crossed with Slco1c1-CreERT2 mice to overexpress Notch1-IC selectively in endothelial cells of the BBB (annotated NotchIC$^{BMECs}$). C57BL6/N mice were purchased from Charles River, France.

Tamoxifen was administered as follows: 100 mg tamoxifen (T5648, Sigma) was suspended in 100 μL ethanol absolute and the solution was mixed well by vortexing. 900 μL peanut oil (P2144, Sigma) was pre-warmed at 55°C. The tamoxifen solution was further mixed in the peanut oil at 55°C and an ultrasonic bath was used to fully dissolve the solution. Tamoxifen was administered p.o. to 12-week-old male mice via feeding needle (Fine Science Tools GmbH) for 3 consecutive days (10 mg/mouse/day). The tamoxifen was maintained at 55°C to prevent recrystallization during administration.

### Cell lines

The immortalized mouse brain capillary endothelial cell (EC) line cEND was described elsewhere.[24] Cells were plated onto a 0.5% gelatin (#G1393, Merck) coated surface and maintained in Dulbecco's modified Eagle's medium (DMEM; #11960044, GIBCO, ThermoFisher Scientific) supplemented with 10% Fetal Bovine Serum (FBS; #P30-3302, PAN Biotech) and 2 mM L-glutamine,

1% penicillin/streptomycin (#15140-122, GIBCO, ThermoFisher Scientific). At confluence, cells were switched to a low serum-containing (2% FBS) differentiation medium.

## METHOD DETAILS

### bacTRAP-based ribosomal profiling of hypothalamic ECs

Affinity purification of translating ribosomes (TRAP) was performed as described previously[26,27] with minor modifications. 12-week-old male and female Slco1c1CreERT2$^{tg/wt}$:ROSA26lSlL10aGFP$^{tg/wt}$ mice were used for the bacTRAP experiment (an equal number of male and female mouse hypothalamic tissue was pooled in each sample). 3 weeks after tamoxifen induction, mice were put either on a CD or an HFD for 3 days. Afterward, mice were sacrificed and the hypothalamus was rapidly dissected using a stainless-steel brain matrix (Agnthos) and immediately frozen in liquid nitrogen. Buffer preparation: Lysis buffer (20mM HEPES [pH 7.4], 5mM $MgCl_2$, 150 mM KCl, 0.5 mM DTT, 100μg/ml cycloheximide, 40U/ml Ribonuclease Inhibitor (Rnasin, Promega) and protease inhibitor [1 tablet of cOmplete mini EDTA-free protease inhibitor cocktail/7 mL and 2 tablets of PhosSTOP/10 mL]); 0.15M KCl IP wash buffer (20mM HEPES [pH 7.4], 5mM $MgCl_2$, 150 mM KCl, 1% NP-40, 0.5 mM DTT, 100 μg/mL cycloheximide); 0.35 M KCl IP wash buffer (20mM HEPES [pH 7.4], 5mM MgCl2, 350 mM KCl, 1% NP-40, 0.5mM DTT, 100 μg/mL cycloheximide). Bead preparation: Dynabeads Protein A (375 μL, Novex, per IP) were washed in 1mL 0.15M KCl IP wash buffer for three times. Afterward, beads were resuspended in 275μL 0.15M KCl IP wash buffer. 50 μg of antibody 19C8 and 50 μg of antibody 19F7 (Cat# Htz-GFP-19F7, RRID: AB_2716736 and Htz-GFP-19C8, RRID: AB_2716737, Memorial Sloan Kettering Monoclonal Antibody Facility) per IP was added into each bead tube. The beads were incubated with slow end-over-end mixing at 4°C overnight. Afterward, the supernatant was removed and the beads were washed in 1mL 0.15 KCl IP wash buffer for 3 three times. After the wash, beads were resuspended in 200μL 0.15M KCl IP wash buffer. Pooled hypothalamic tissue (4 pooled mice per sample; 4 samples per group) was homogenized on ice with lysis buffer (1mL per sample) at 4°C. Homogenates were transferred to low binding microcentrifuge tubes (Nonstick, RNase-free microfuge tubes,1.5 mL, Ambion, Invitrogen) and centrifuged 10 min, 2000g at 4°C to obtain the post-nuclear supernatant. The supernatant was transferred to a new tube on ice, and 1/9 sample volume of 10% NP-40 (final concentration: 1%) and 1/9 sample volume of 300 mM DHPC (final concentration: 30 mM) were added. This solution was mixed, incubated on ice for 2 min and then centrifuged at 17,000 g for 10 min at 4°C. The resulting supernatant was transferred to a new tube and a 25 μL aliquot was removed, transferred to a new tube, flash frozen in liquid nitrogen and stored at −80°C for purification as input RNA. 200 μL of antibody-bound beads were added (800–1000 μL supernatant) and incubated at 4°C for 1 h with end-over-end mixing. Beads were collected with a magnet and resuspended in 1 mL 0.35 M KCl IP wash buffer. Beads were washed three more times with 1mL of 0.35 M KCl IP wash buffer. After the final wash, the beads were collected with a magnet and the supernatant removed. The RNA was eluted by the addition of buffer RLT (350 μL) to the beads, allowed to incubate at room temperature (RT) for 5 min and RNA was subsequently purified using the RNeasy Micro Kit (#74004, QIAGEN). RNA integrity was assessed using an Agilent 2100 bioanalyzer.

### RNA bulk sequencing

Pre-amplification using the Ovation RNASeq System V2 was performed. Total RNA was used for first strand cDNA synthesis, using both poly(T) and random primers, followed by second strand synthesis and isothermal strand-displacement amplification. For library preparation, the Illumina Nextera XT DNA sample preparation protocol was used, with 1 ng cDNA input. After validation (Agilent 2200 TapeStation) and quantification (Invitrogen Qubit System) all 24 transcriptome libraries were pooled. The pool was quantified using the Peqlab KAPA Library Quantification Kit and the Applied Biosystems 7900HT Sequence Detection and sequenced on an Illumina NovaSeq S2 flowcell with a PE100 protocol. The RNA sequencing pipeline utilizes the GRCm38 assembly of the mouse genome as gene sets from Ensembl release 96.[28] We applied the community-curated nf-core/rnaseq analysis pipeline version 1.4.2 [29] for processing RNA-sequencing data. Gene-level quantification was performed using Salmon 0.14.1 [30] with the GRCm38 reference genome. Differential gene expression analysis was conducted using the DESeq2 1.26.0 R package.[31]

### *In situ* hybridization

Anesthetized mice were perfused with PBS (pH 7.4) followed by 4% PFA dissolved in PBS (pH 7.4). Brains were removed from the skull, post-fixed in 4% PFA at 4°C overnight, then moved to 20% sucrose solution (in 1X PBS) at 4°C until cutting. 20 mm thick sections were generated with a cryostat.

Detection of Pecam1 or Notch1 mRNA was performed using a fluorescent *in situ* hybridization technique (RNAscope, Advanced Cell Diagnostics) according to the manufacturer's instructions. 3-plex negative and 3-plex positive control probes were processed in parallel with the target probes. Sections were mounted on SuperFrost Plus Gold slides (ThermoFisher), dried at RT, briefly rinsed in autoclaved Millipore water, air dried and baked at 60°C overnight. Afterward, slides were submerged in Target Retrieval (Cat No. 322000) at 95.0°C–99.0°C for 8min, followed by a brief rinse in autoclaved Millipore water and dehydration in 100% ethanol. A hydrophobic barrier was then created around the sections using an ImmEdge hydrophobic barrier pen (Cat No. 310018). All incubation steps were performed at 40°C using the ACD HybEz hybridization system (Cat No. 321462) according to the manufacturer's instructions. Sections were incubated with Protease III (Cat No. 322340) for 30 min. The subsequent hybridization, amplification and detection steps were performed according to the manufacturer's instructions (Multiplex Fluorescent Detection kit v2, Cat No. 323110). For simultaneous detection of genes within the experiment, the Pecam1 probe was combined with the fluorophore Opal 520 (Dilution

1:750), while the Notch1 probe was combined with the fluorophore Opal 650 (Dilution 1:750). After the treatment sections were mounted with DAPI using Vectashield Antifade Mounting Medium (Vector Laboratories), covered using a coverslip and stored at 4°C in the dark until imaging.

Images were acquired with a confocal Leica TCS microscope, using the 40x/1.30 immersion objectives. Laser intensities for the probe channels were kept constant throughout the imaging process. Images of the PVN were captured from rostral to caudal, rendering approximately 5–6 sections per animal. Images were imported into Fiji ImageJ (NIH), where DAPI and Pecam1 probe channels were adjusted regarding brightness and contrast. The mouse brain atlas published by Paxinos and Franklin was used as a reference to identify the ROIs. Cells stained for the respective target were manually quantified. DAPI signal served as a marker for individual cells, while Pecam1 positive cells were identified by overlap of DAPI and Pecam1. Colocalization of Pecam1 and Notch1 was determined by manually counting individual Notch1 positive cells.

### Western blotting

For assessment of Glut1 expression, 80μL RIPA buffer (150mM NaCl, 1% NP-40, 0.5%sodium deoxycholate, 0.1% SDS, 50mM Tris-HCl) supplemented with Protease Inhibitor Cocktail (cOmplete Roche) was added into each well of cultured cEND cells. Adherent cells were scraped off the plates and lysates were rotated at 4°C for 20min, then centrifugated at 4°C, 17,000rpm for 25min. The supernatant was recovered and the protein concentration was measured by a BCA protein assay kit (Pierce BCA Protein Assay, # 23225, Thermo Fisher Scientific). Samples were prepared by mixing lysates and Laemmli buffer, the mixture was heated at 70°C for 5 min, then loaded onto NuPAGE 4 to 12%, Bis-Tris, 1.5 mm, Mini Protein Gel (NP0336box, Invitrogen), the gels were run in the NuPAGE MOPS SDS running buffer at 180V for 50minutes, then protein was transferred to PVDF membranes by Trans-Blot Turbo Transfer System (Bio-Rad). The membranes were blocked by 5% milk (Nonfat dried milk powder; #A0830,0500, PanReac AppliChem) in TBS and incubated overnight at 4°C with the primary antibodies: anti-Glut1 (1:1000, #07–1401, Merck Millipore), Anti-Calnexin (1:10,000, #208880, Merck Millipore).

### Measurement of glycolytic flux

The extracellular acidification rate (ECAR) was measured by Seahorse XF96 Analyzer (Agilent). 30,000 cells were seeded into each assay well, when cells had reached confluency, the medium was changed to 2% FCS for 24h. For mouse serum treatment, cells were treated with a culture medium supplemented with either 10% of serum obtained from mice, which were fed CD for 3 days or 10% of serum obtained from mice fed an HFD for 3 days for 24h. For Notch activation, recombinant mouse Dll4 protein (#1389-D4, R&D) was added at 1μg/mL. During the measurement, the cells were changed to assay medium (pH 7.4) and transferred to a $CO_2$-free incubator and maintained at 37°C for 1 h before starting the assay. Initial measurement cycles were performed to obtain the basal ECAR. Afterward, the cells were treated sequentially by a saturating concentration of 100mM glucose, 1μM oligomycin and 100 mM 2-desoxyglucose (DG) (Seahorse XF Glycolysis Stress Test Kit; #103020-100, Agilent) according to manufacturer's instructions.

### Analysis of mouse serum

Serum total cholesterol and free cholesterol levels were detected using the Cholesterol Quantification Kit (#MAK043, Sigma) according to the manufacturer's instructions. Serum lipid peroxidation levels were measured using a Lipid Peroxidation (MDA) Assay Kit (#MAK085, Sigma), which determines the lipid oxidation end product malondialdehyde (MDA) in serum according to manufacturer's instructions.

### Immunohistochemistry

For immunohistochemical analyses, mice were anesthetized and perfused transcardially with phosphate-buffered saline (PBS) followed by freshly prepared 4% paraformaldehyde (PFA). The brains were immersion fixed overnight at 4°C, followed by dehydration in 30% sucrose in PBS for 2–3 days (if not stated otherwise). Afterward, the brains were frozen at −80°C and 30um thick sections were cut on a cryostat. Brain sections were washed (3 × 10 min) with PBS 0.1 M (pH 7.4) and incubated in a blocking solution (PBS containing 0.25% Triton X-100 and 3% goat serum) for 1 h at RT. Primary and secondary antibodies were diluted in a blocking solution. Sections were incubated with the primary antibody overnight at 4°C, washed with PBS and incubated with the secondary antibody for 1 h at RT, protected from light. Primary antibody used was anti-Glut1 (#ab652, Abcam). Secondary antibody used was Alexa Fluor 488 goat anti-rabbit (1:500, #A11008, Abcam). Fluorescein-conjugated *Lycopersicon esculentum* lectin (1:200, #FL1177, Vector Laboratories) was used to visualize brain microvessels.

The signals of fluorescently labeled insulin (AF488-insulin) were amplified via immunohistochemical staining against the fluorescent tag Alexa Fluor 488 (1:500, #A11094, ThermoFisher Scientific). Free-floating immunohistochemistry was performed on all brain sections. In between steps, sections were washed in PBS. Briefly, brain slices were rinsed (2 × 10min) in PBS, washed and then incubated in 0.3% glycine for 10 min, followed by 0.03% SDS for 10 min. Sections were incubated in 3% donkey serum blocking solution for 1 h at RT. The sections were incubated with primary antibody overnight at RT and then washed 3 × 10 min. Afterward, the sections were incubated with secondary antibody Alexa 594 (1:400, #A21207, ThermoFisher Scientific) overnight. Brain slices were then mounted on glass slides (SuperFrost, ThermoFisher Scientific) with Vectashield (Vectorlabs).

The immunohistochemical staining of pAKT was performed on brain slices of AF488-insulin-infused mice. Free-floating immunohistochemistry was performed on all brain sections. In between steps, sections were washed in 0.05% Tween 20 in Tris-buffered saline. Briefly, brain slices were rinsed in Tris-buffered saline for 5 min, washed and then incubated in 1% $H_2O_2$ for 30 min. Sections were blocked with TNB blocking buffer, consisting of 0.1 M Tris-HCl, pH 7.5, 0.15 M NaCl and 0.5% (w/v) Blocking Reagent (# FP1020, PerkinElmer). Afterward, the slices were incubated with pAKT primary antibody (1:500 in TNB buffer, #4060, Cell Signaling) overnight at RT. HRP-labelled anti-rabbit-IgG (#NEF812E001EA, PerkinElmer) antibody and DAPI (1:1,000, #62248, ThermoFisher Scientific) were applied on sections for 30 min at RT. Immunocomplexes were revealed with Cy3 fluorophore by incubation for 3 min in amplification buffer (1:100, PerkinElmer). Brain slices were then mounted on glass slides (SuperFrost, ThermoFisher Scientific) with Vectashield (Vectorlabs).

To ensure comparable immunostaining within an experiment, sections were processed in parallel under identical conditions.

## Positron emission tomography (PET) scanning

PET imaging was performed using an Inveon preclinical PET/CT system (Siemens). Mice were anesthetized with 2% isoflurane in 65%/35% nitrous oxide/oxygen gas and positioned on a dedicated mouse carrier (MEDRES, Germany) carrying two mice. Body temperature was maintained at 37.0 ± 0.5°C by a thermostatically controlled water heating system. For injection of the radiotracer, a catheter consisting of a 30G cannula connected to a polythene tubing (ID = 0.28 mm) was inserted into the tail vein and fixed by a drop of glue. After starting the PET scan, 7–8 MBq of [18F]FDG in 50–100 μL saline were injected per mouse. Emission data were acquired for 45 min. Thereafter, animals were automatically moved into the CT gantry and a CT scan was performed (180 projections/360°, 200 ms, 80kV, 500μA). The CT data were used for attenuation correction of the PET data and the CT image of the scull was used for image co-registration. Plasma glucose levels were determined from a tail vein blood sample using a standard glucometer (Bayer) after removing the tail vein catheters. PET data were histogrammed in time frames of 12 × 30s, 3 × 60s, 3 × 120s, 7 × 240s, rebinned in 3D, and images were reconstructed using the MAP- SP algorithm provided by the manufacturer. For co-registration the imaging analysis software Vinci was used.[32] Images were co-registered to a 3D mouse brain atlas constructed from the 2D mouse brain atlas published by Paxinos.[33]

### *Kinetic modeling*

An image-derived input function was extracted from the PET data of the aorta, which could be identified in the image of the first time frame of each animal. Input function data were corrected for partial volume effect by assuming a standardized volume fraction of 0.6.[34] Parametric images of the [18F]FDG kinetic constants K1, k2, k3, and k4 were determined by a voxel-by-voxel (voxel size = 0.4 mm × 0.4 mm x 0.8 mm) fitting of data to a two-tissue-compartment kinetic model. K1 is the constant for transport from blood to tissue, k2 for transport from tissue to blood, k3 the constant for phosphorylation of [18F]FDG to [18F]FDG-6-phosphate, and k4 the constant for dephosphorylation. As a measure for glucose transport to the brain, parametric images of brain tissue glucose divided by the plasma glucose concentration ($C_E/C_P$) were calculated taking into account the different efficiencies of [18F]FDG and glucose, a method that is insensitive to changes of the lumped constant:

$$C_E/C_P=K_1/(k_2+k_3/0.26)$$

Note, that since cellular activation is accompanied by increased glucose transport, $C_E/C_P$ is also a surrogate for cellular activity.

### *Statistics*

Statistical testing was performed by application of a voxel-wise t test between groups. 3D maps of *p*-values allow for the identification of regions with significant differences in the parameters. From these regions we defined volumes of interest (VOIs) and performed additional statistical testing for these VOIs. For presentation only, 3D maps of *p*-values were re-calculated on a 0.1 mm × 0.1 mm x 0.1 mm grid from the original dataset using trilinear interpolation.

## Electron microscopy imaging

Hypothalami of the indicated mouse lines were dissected, cut into cubes (1 × 1 × 1mm) and directly fixed in 2%GA, 2%FA in 0.1M CaCodylate buffer for 48h. Afterward, samples were rinsed in 0.1 M cacodylate buffer (pH 7.2) and incubated in 2% OsO4 in 0.1 M cacodylate buffer (pH 7.2) for 2 h at 4°C. Tissues were dehydrated using ascending ethanol series, transferred to propylene oxide and finally embedded in epoxy resin for 72 h at 62°C. Ultrathin sections (70 nm) were cut with a diamond knife (Diatome, Biel, Switzerland) on an ultramicrotome (EM-UC6, Leica Microsystems) and placed on copper grids. Sections were contrasted with 1.5% uranyl acetate and lead citrate (Reynolds solution). Images were acquired with a transmission electron microscope (JEOL JEM 2100Plus), camera OneView 4K 16bit (Gatan), and software DigitalMicrograph (Gatan) at 80 kV at room temperature.

## Blood-brain barrier permeability assay

Experimental mice received a tail vein injection of 10-kDa dextran tetramethylrhodamine (10 mg/ml, 10μL/g body weight; #D1817, Thermo Fisher Scientific). 15 min after injection, brains were dissected and fixed by immersion in 4% PFA at 4°C overnight. After 24h in 30% sucrose, 30μm sections were prepared and co-stained with fluorescein-conjugated *Lycopersicon esculentum* lectin (#FL-1171, 1:200, Vector Laboratories) to visualize brain microvessels.

### Fluorescently labeled insulin injection and imaging

Experimental mice were fasted overnight for 16h and anesthetized. Fluorescently labeled insulin (AF488-labelled insulin; 250 nmol/kg; Novo Nordisk) was infused into the *Vena cava* and allowed to circulate for 15 min. In order to retain fluorescence signal and avoid over-fixation, the 4% paraformaldehyde (PFA) was briefly perfused for 1 min (~10 mL). After post-fixation, brain specimens were cut into cryostat sections, collected in an anti-freeze solution (30% ethylene glycol and 20% glycerol in PBS) and processed for immunohistochemistry.

### Intraperitoneal insulin tolerance test

Intraperitoneal insulin tolerance tests (ipITTs) were performed in random fed mice. Two hours before starting the experiment, food was removed and bedding was renewed. Blood glucose concentrations were measured from tail vein samples using a handheld glucometer (Contour, Bayer HealthCare, Germany). Mice received an intraperitoneal injection of 0.75 U/kg body weight of human insulin (Huminsulin Normal 100, Lilly) and blood glucose concentrations were measured at baseline, 15, 30 and 60min after insulin administration.

### Indirect calorimetry

Indirect calorimetry was performed using an open-circuit, indirect calorimetry system (PhenoMaster, TSE systems). Mice were placed in training cages for three days before data acquisition to adapt to the pellet and liquid dispensers of the system. After data acquisition, mice were returned to their home cages. For the measurement mice were placed in regular type II cages with sealed lids at room temperature (22°C) and allowed to adapt to the chambers for at least 24 h. Food and water were provided *ad libitum*. All parameters were measured continuously and simultaneously.

## QUANTIFICATION AND STATISTICAL ANALYSIS

For quantitative analyses, littermates were used. Data presentation with scatter dot plot graphs includes values of individual data points. All values were expressed as mean ± SEM unless otherwise indicated. Statistical analyses were conducted using GraphPad PRISM (version 9.1.0). Detailed information on statistical analyses is provided in the figure legends and the methods section. Datasets with only two independent groups were analyzed for statistical significance using an unpaired two-tailed Student's t-test, and two dependent groups were analyzed by paired two-tailed Student's t-test. Datasets with more than two groups were analyzed using one-way ANOVA with the Tukey post hoc test. two-way ANOVA with Šídák post hoc test was used for grouped analysis. Statistical significance was determined based on p values as follows: $*p < 0.05$, $**p < 0.01$, $***p < 0.001$ and ns - not significant.